Dependencies of Optical Properties on the Thickness of SnO₂ Thin Layers Grown with CSP Method

Harakat Mohsin Roomy^a, Dawood Salman Abd Al-Kader^{b*} and Abdulaziz Mahmood Ahmed^b

^aMinistry of Education, Baghdad, Iraq ^bMinistry of Education, Directorate in Al Anbar, Iraq

(received July 23, 2024; revised September 28, 2024; accepted October 24, 2024)

Abstract. Optically transparent oxide thin layers have been the subject of considerable interest over the past century due to their potential applications. As a result, the development of thin films with high optical transparency has been a prominent area of investigation. SnO₂ represents a significant member of the oxide materials family, exhibiting exceptional optical transparency across a broad range of the electromagnetic spectrum and low electrical resistance. In this study, the optical properties of pure SnO₂ thin layers were investigated. For this purpose, different thicknesses (510, 630, 770 and 940 nm) prepared by chemical spray pyrolysis (CSP) technique and deposited on glass substrates at 400 °C. Within the visible-region, the SnO₂ films exhibited a high optical transmittance of "85-90%", it was observed that an increase in thickness of the thin layers resulted in a reduction in band gap, high absorbance and low transmittance. For wavelength (330-900 nm) the following parameters were calculated: absorption coefficient, index of refraction, constants of real and imaginary dielectric, extinction coefficients, optical conductivity and energy gap for all types of optical electronic transitions by using Shimadzu UV-2450 spectrophotometer.

Keywords: SnO₂, thin layer, CSP method, thickness, optical properties

Introduction

According to recent studies, basic and applied research has shown a great deal of interest in silica-based nanomaterials. These materials can be produced with a wide range of pore sizes, shapes and sizes. Additionally, the surface characteristics of these materials can be readily modified for various applications contingent upon the synthesis and functionalization procedures employed (Nayl, 2022). Certain metal oxide compounds, whether in their pure form or doped with other materials, are frequently utilized in thin film technology in materials engineering (Paliwal and Sharma, 2014). A type of material known as a transparent conducting coating possesses both good optical transmission at visible wavelengths and strong electrical conductivity (Zhang and Yongming, 2021). Transparent conducting oxide materials are found in many everyday objects. Most of these applications involve thin-film solar photovoltaics (Torre Pari and Aquino, 2023), smart windows (Brunin and Ricci, 2022), (organic) light-emitting diodes (OLEDs) and display technology (Yan and Zhang, 2015). SnO₂ is a member of a significant family of oxide materials that exhibits exceptional optical transparency in the part of the electromagnetic spectrum that is observable along with low electrical resistance (Sarmah and Kumar, 2010). The metal oxide SnO₂ is

of particular interest due to its enormous bandgap of "3.6 eV" and wave-length (λ) of further than "0.4 μ m" and its variations are related to the deposition technique used (Abdullah and Al-Taay, 2021), that strong optical and electrical qualities are correlated with good chemical and mechanical stability (Kumar and Kaphle, 2023). Hence, despite the large energy gap in these thin films, the optical transmittance spectrum spans (400-1500) nm, depending on the material preparation parameters. Furthermore, the potential for free electrons to exist during beam conduction (Erken et al., 2018). Various techniques have been used to prepare films, including spray pyrolysis, sol gel, chemical and physical vapor deposition but chemical spray pyrolysis "CSP" has a few key advantages over other methods, including the ability to deposit over large areas, good reproducibility, chemical homogeneity in the final product, easy doping material addition and a high film growth rate. It also requires simple and inexpensive equipment. The thicknesses of these films range from 0.1 to 10 µm and can be either dense or porous (Chen and Wang, 2013). In this study, a pyrolysis spraying process to analyze the optical properties of tin oxide thin layers deposited on glass substrates. The objective was to develop a film with excellent physical characteristics within the visible range. The study focused on determining the exact influence of thickness on these properties.

^{*}Author for correspondence; E-mail: dawodalany@gmail.com

Materials and Methods

The synthesis of tin oxide utilized tin tetrachloride penta-hydrate (SnCl₄.5H₂O) and deionized water. Spray pyrolysis works on the basis of the pyrolytic breakdown of the salts of the material that is to be deposited. Its primary components are an airtight fiber chamber, a hot plate, a liquid level monitor, a rotor for the spray nozzle and a gas regulator value. Air was used as gas carrier and the spraying flow rate has been adjusted to approximately 4 mm/min. The schematic diagram for the homemade spray pyrolysis system is displayed in Fig. 1 and selected parameter in Table 1. Pieces measuring 5 cm by 1 cm were cut from glass substrates with 90% transmittance. Prior to deposition, the substrates of glass were cleaned in an ultrasonic bath with deionized acetone for 10 min, followed by ethanol for 10 min and finally with deionized water for 10 min. Substrates were then dried by blowing air and wiped with optical soft tissue before using for film deposition. In order to achieve the best possible uniformity of the film and efficient heat transfer, a clean glass slide is placed on a smooth, flat surface that serves as a thermal conductor. To ensure proper adhesion and thin film quality, heat

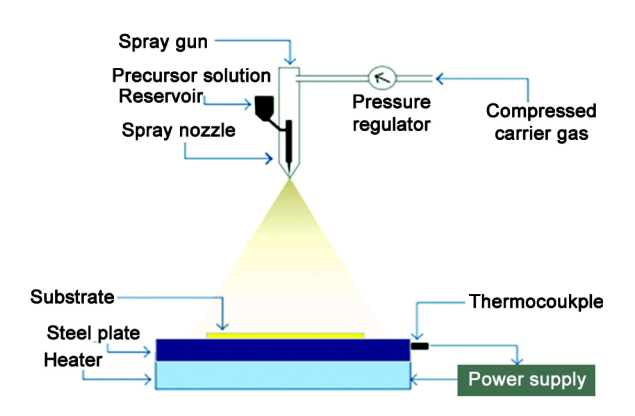


Fig. 1. The scheme of the CSP setup.

Table 1. Selected method parameters CSP of thin layers

Parameters of spray	Optimal value/item			
Nozzle	"glass"			
Nozzle-substrate distance	"25" cm			
(SnCl ₄ .5H ₂ O) concentration of solution	"0.1" M			
Solvent	Purified water			
Gas pressure	3.5 Bar			
Flow rate of solution	"4" mL/min			
Carrier gas	Compressed of air			
Temperature of substrate	"400" °C			

the substrates to the appropriate deposition temperature, typically 400 °C. The distance from the nozzle to the glass substrate was approximately 25 cm and the air pressure used was 3.5 bars. Tin oxide was synthesized using the spray pyrolysis technique, with 0.1 M of Tin tetrachloride pentahydrate (SnCl₄.5H₂O with purity of 100%) being utilized. The precursor was mixed with the required volume of deionized water and stirred (using the ARGO LAB M2-A magnetic stirrer) for about 15 min to be sure that the mixture solutions are mixed properly. With the spray nozzle, atomize the precursor solution. The air carrier gas aids in transporting the tihinny droplets to the heated substrate. Tin oxide thin films are formed when the precursor droplets undergo pyrolytic decomposition upon contact with the heated substrate. The solvent evaporates, leaving behind a solid film. Improve the crystallinity and thin film qualities by annealing the deposited films for 1.5 h at 400 °C in oxygen. The thickness of the prepared layers was determined using the weighing method.

Using a UV-VIS spectrophotometer, the spectrum for transmittance and absorbance measurements was obtained in the 300-900 nm wavelength range.

Results and Discussion

In Fig. 2a the absorption spectra of SnO, thin layers at various thicknesses are shown. Although variations in absorbency were noted, it was noted that the curves' forms were similar, particularly in the UV- area with a wave-length of 350 nm. The absorption spectra showed comparatively poor absorbency due to thicker thin films. For extended wavelength ranges, all thin layers exhibit low absorption. The region of the spectrum with large wave lengths, where effects of interference occur, is where the thickness effect is observed. Fig. 2b illustrates how the transmittance (T) spectra of tin oxide thin films with vary thicknesses (510, 630, 770 and 940 nm) varies with photon wavelength. It is evident that as the thickness rises, the films' transmittance decreases. This results from a drop in light scattering losses. The average transparency in the visible range is around ~87%. The graphic shows that at 500 nm wavelength, transparency decreases with increasing film thickness from 90% to 80%. Such transmission behavior could be described by particular defect subsystem modifications that occur through the deposition of SnO₂ films. Each film has a low transmittance in the ultraviolet area, which increases as the wavelength moves toward the near-infrared. Furthermore, the films exhibited a distinct interference Optical Properties of SnO, 273

pattern in the transmittance manifests, a sign of improved homogeneity and high quality. These outcomes were fairly consistent with the findings of (Susilawati and Muliyadi, 2020). The SnO₂ thin layer's Spectrum of Reflection R was obtained by utilizing the T and A data of the thin layers. (Billur and Gencosman, 2020):

$$T=(1-R)^2e^{-A}$$
....(1)

Figure 2c shows the reflectance spectra of thin layers as a function wavelength for SnO₂. It has been noted that thicker films exhibit increased reflection in the visible and near-infrared spectrum. The reflectance values were detected between 0.05% and 0.1% at 500 nm wavelength. It is evident that a 510 nm-thick film exhibits high transmittance throughout the electromagnetic spectrum's ultraviolet, visible and infrared areas. In contrast, it is discovered that the film's reflectance is observed to be low in the aforementioned regions. As a result, the layers high transmittance and low reflectance qualities make it a suitable material for antireflection coatings as well as solar thermal applications. These outcomes were quite similar to the ones attained by (Lei Ma and Hao, 2002).

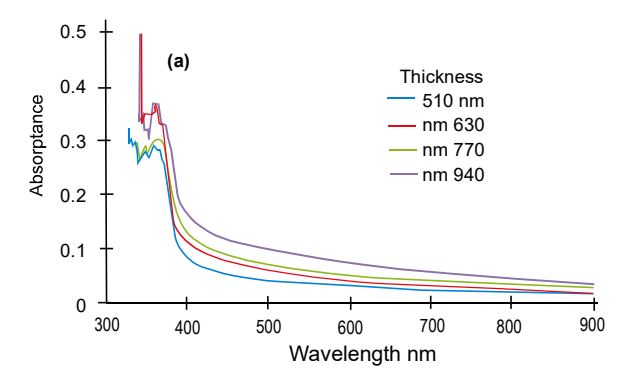
The optical absorption coefficient (α) in the 300-900 nm wavelength range is presented in Fig. 2d. Thicker films exhibit a higher α value in the forbidden gap region compared to thinner layers, as indicated by the results. According to the absorption spectra, the manner in which α behaves similarity to the absorption. It is evident from Fig. 2a that when the thickness of the thin layer's increases, the absorption coefficient of the SnO₂ films decreases. It is also evident that the absorption coefficient has high values at high photon energies, which may support the idea that an electron transition occurs directly. These results were somewhat comparable to those obtained by (Susilawati and Muliyadi, 2020).

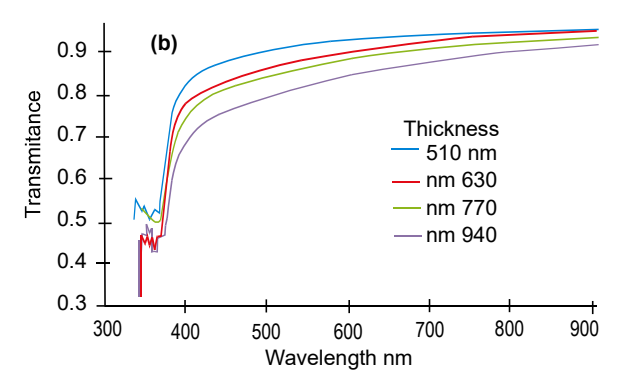
Nearby the edge of absorption, the optical energy-gap and the absorption coefficient α are connected. Using Taucs relation as an example, the power-law behavior appears as follows: (Khamee and Niyom, 2023).

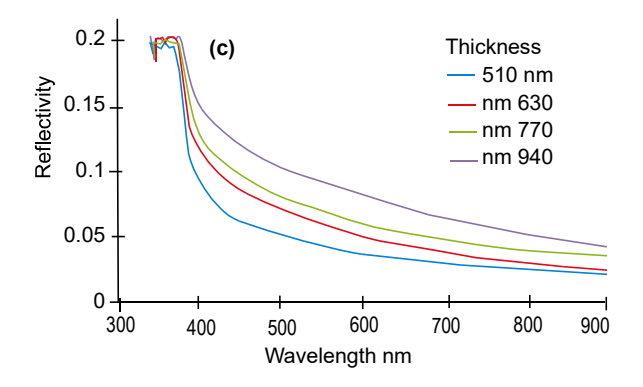
$$\alpha h \upsilon = A (h \nu - E g)^r....(2)$$

r equal to "1/2" - Direct of allowed transition r equal to "2" - Indirect of allowed transition where:

" α " is the coefficient of absorption, " ν " is the incidents







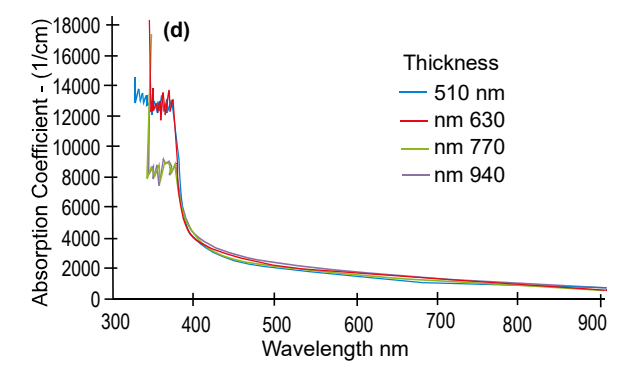


Fig. 2. Variation in the optical: (a) Absorptance (b) Transmittance (c) Reflectivity (d) Absorption coefficient with wavelength of SnO₂ layers at different thickness.

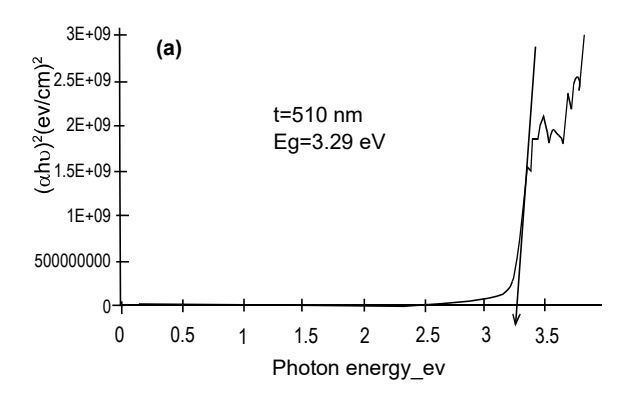
of photon's frequency, "h" is the Planck constant, "A" is a constant, "E_g" is the optical band gap and the index "r" could have various values depending on the electronic transition.

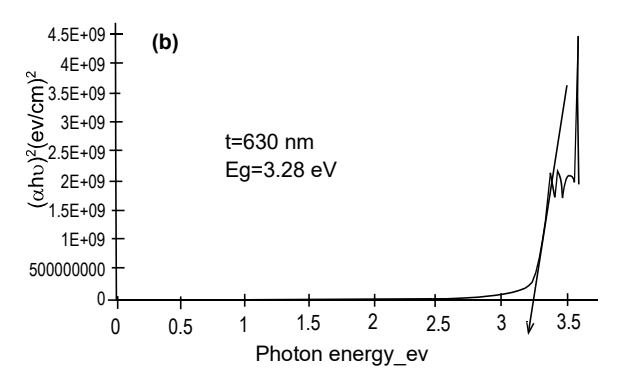
The computed optical band gap is shown in Fig. 3 and is tabulated in Table 2. As explained in Fig. 3, the direct band gap of the SnO2 thin layers was obtained by extending the $(\alpha hv)^2$ straight line against the (hv) plot to α =0. Thus, the original band gap was decreased from 3.29 to 3.21 eV with growing in thickness. The optical band gap of the thin layers deposited does not differ considerably with the thickness of the thin layers. However, the gap decreases slightly with increasing thin layer' thickness which agrees with previous reports (Carreno and Rangel, 2003). The diminution in the band gap may be explained by the fact that the light beam transmittance typically decreases and shifts toward higher wavelengths as the thin film thickness increases, and consequently, the optical gap energy decreases as the optical absorption edge approaches longer wavelengths (lower photon energies). Moreover, this difference can be attributed to the metal particles that created surface flaws in the SnO₂ crystallites. In fact, the lattice degree structure and thermal disorder in the testers regulate the optical band gap (Korber and Harvey, 2008). As a result, the increase in layer thickness may cause the crystalline state to deform significantly, indicating changes in the electrical stability.

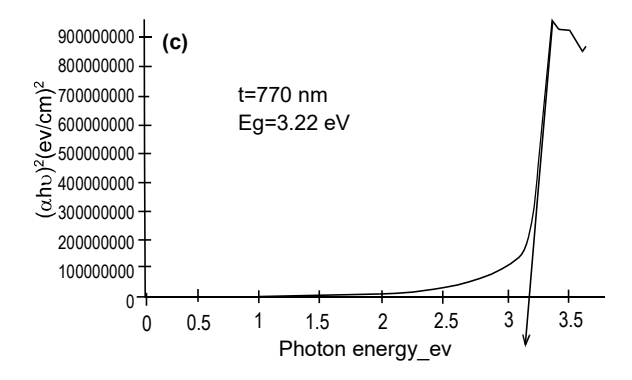
In Fig. 4, the indirect band gap energies are plotted against the film thickness of SnO₂ layers. It is evident from the figure that there is a slight change in the value of the gap energies as the film thickness increases. The indirect band gap energy decreases from 3 eV to 2.9 eV with the greater thickness of the film. This decrease in the energy gap values is attributed to the improved crystallization with the greater thickness of the film.

Table 2. Variations in the energy (eV) for allowed direct besides indirect electronic transitions of SnO₂ thin films with varying thicknesses

Thickness (nm)		Energy- gap (eV) Indirect allowed	Urbach energy (eV)	
510	3.29	3	1.2	
630	3.28	3.1	1.25	
770	3.22	2.88	1.26	
940	3.21	2.9	1.27	







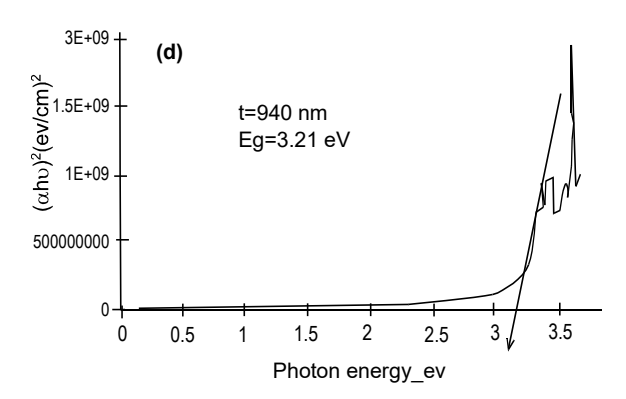
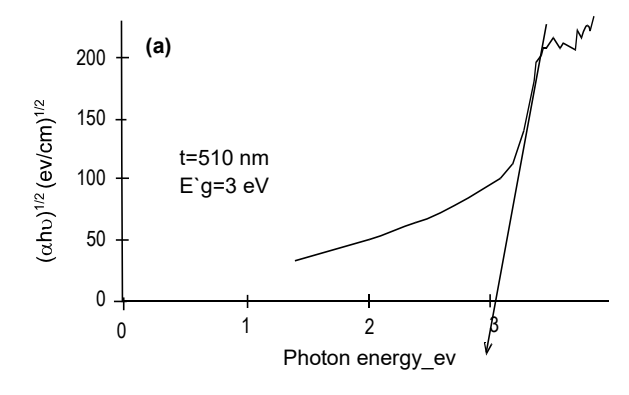
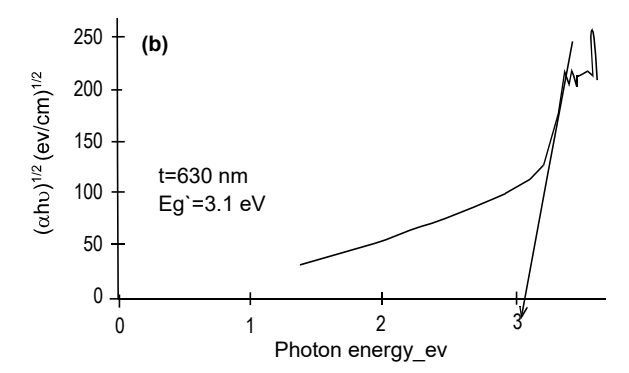
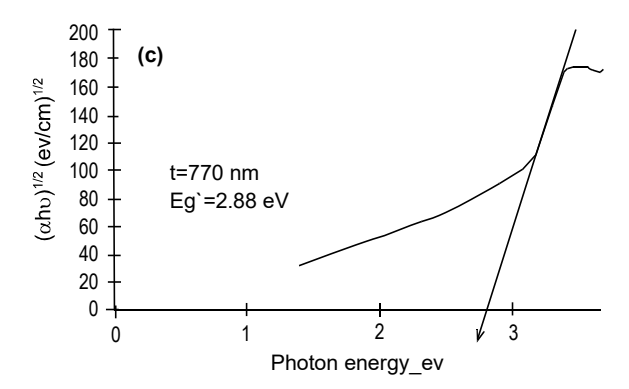


Fig. 3. The allowed direct electronic transitions of SnO₂ thin films with different thicknesses.

Optical Properties of SnO, 275







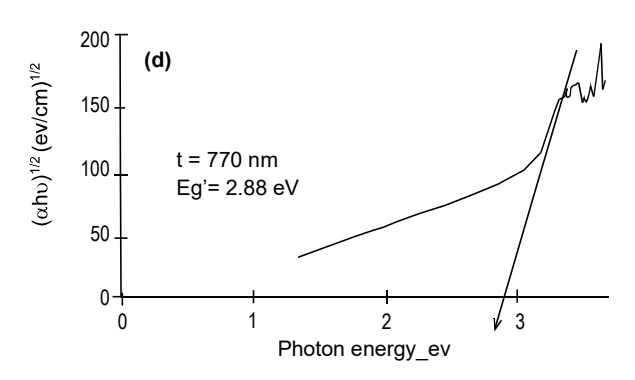


Fig. 4. The allowed indirect electronic transitions of SnO₂ thin films with different thicknesses.

The amount of light absorption is related to the index of refractive "n" and the frequency of light absorption is related to the coefficient of extinction (k). Determining the "n" indices of materials is crucial, particularly for materials that can be used to create any kind of optical device, such as switches, filters and modulators. By applying relation (3), (n) can be derived from the reflectance (R). (Yadav et al., 2009):

$$n = \left[\left(\frac{1+R}{1-R} \right)^2 - (K_o^2 + 1) \right]^{1/2} + \frac{1+R}{1-R} \dots (3)$$

The values of (n) for various thicknesses of SnO, thin layers are shown in Fig. 5a. The (n) values are greater in the UV-visible range and lower in the N-IR wavelength. This suggests that the film exhibits a markedly high rate of light slowing in the UV-region followed by a rapid decline to a relatively low rate in the NIR region. It has been demonstrated that rising the thickness results in a corresponding rise in the refractive index. This phenomenon can be attributed to a general enhancement in reflectance as the thin layer thickness rises. This result can be explained by the fact that when thin films become thicker, the light beam's angle of refraction within the thin film material decreases, which increases the optical refractive index. The coefficient of extinction "k" can be computed from the absorbance data A as follows (Farva and Kim, 2021):

$$K = \frac{\alpha \lambda}{4\pi} \dots (4)$$

where:

(α) The optical absorption coefficient

As shown in (Fig. 5b), the (K) of the SnO_2 thin layer increases with rising wavelength and decreases with increasing thickness. This is a result of reducing the absorption coefficient by increasing the thickness. Fig. 5c and d displays the constant's of dielectric real and imaginary parts " ε_1 and ε_2 ". The behavior of ε_1 has a similarity to that of the "n" due to the smaller value of k_2 when compared to n, whereas ε_2 is mostly dependent on k values, which are associated with variations in the absorption coefficient. Consolidated optical properties of SnO_2 over the Vis-spectral region at 550 nm wavelength results included in Table 3.

An exponential portion that can be seen around the optical band-edge and along the coefficient of absorption curve referred to as the "Urbach tail". This exponential

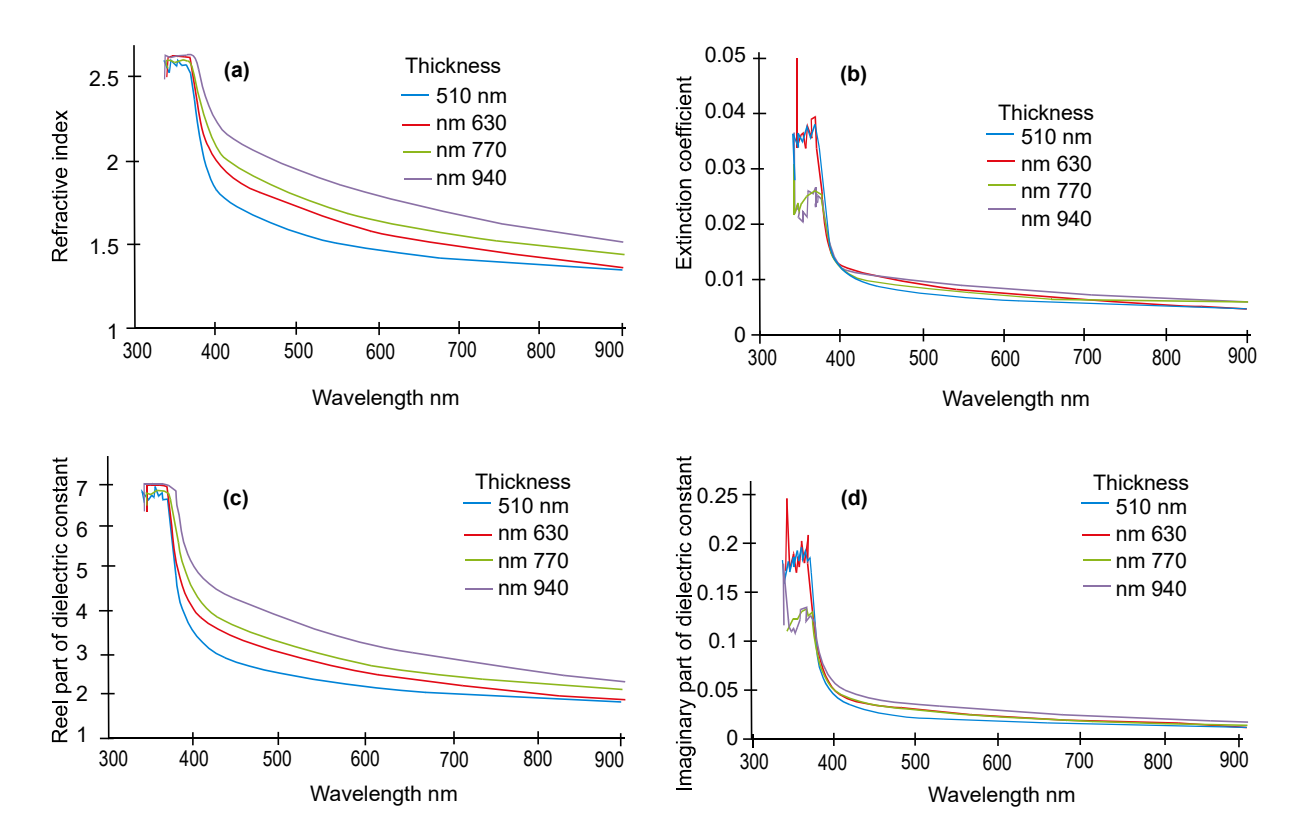


Fig. 5. Variation in the (a) Refractive index (b) Extinction coefficient (c) Real and imaginary part dielectric constant with wavelength (nm) of SnO₂ layers at different thickness.

tail in materials with weak crystallinity and disorder as well as amorphous materials, due to their localized states extending into the band-gap. The following equation represents the Urbach empirical rule, which describes the spectral dependency coefficient of the absorption " α " and photon energy "hv" in the low photon energy region (Hassanien and Akl, 2015):

$$\alpha = \alpha_o exp(\frac{h\nu}{E_u})....(5)$$

where:

" α_o " is a constant and " E_u " represents Urbach energy. The tail width could be determined by graphing "Ln(α)" as a function of "hv". " E_u " in the energy-gap. The value of E_u was then extracted from the reciprocal slope of the linear component, according to Fig. 6a. The localized conditions and defect levels in the energy-gap were thought to be the causes of the increased E_u values with increasing thickness. The consolidated experimental results included in Table 3. The electromagnetic wave's reduced amplitude after passing through a thickness is represented by the skin depth(s), which may be computed

using the following relation:

$$S=\lambda/4\pi\kappa$$
....(6)

Figure 6b shows the plot of the skin depth vs. wavelength for various thicknesses. This figure, clearly shows the increase in skin depth with increasing wave length and the slight variation with increasing thickness of the SnO_2 thin layers. The optical conductivity (σ_{opt}) is estimated using absorption coefficient (α) as follows (Zhang and Yongming, 2021):

$$\sigma_{\text{opt}} = \left(\frac{\alpha nc}{4\pi}\right)$$
(7)

where:

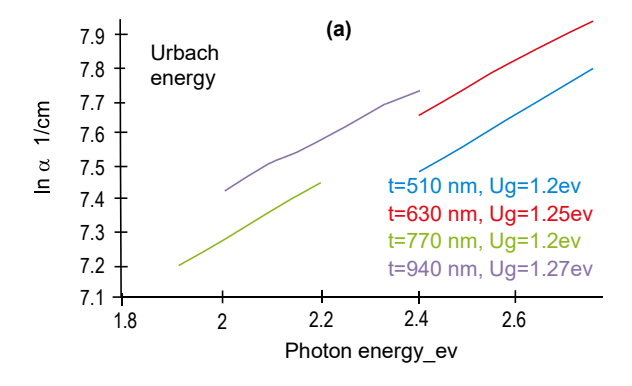
"c" is the v of light velocity

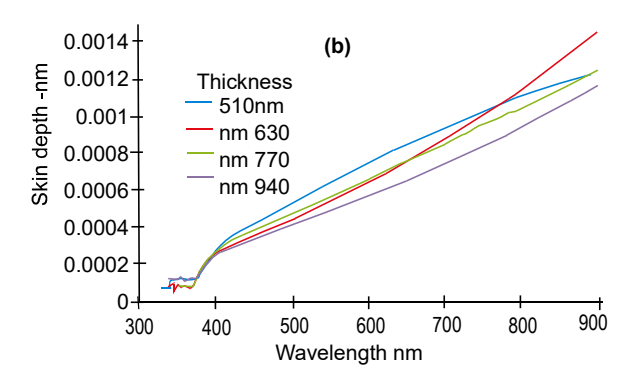
The (σ_{opt}) , decreases and then increases with increasing photon energy (Fig. 6c). In addition, it changes un sequenced with increasing thickness. The increase in the absorption coefficient and the possibility of electron excitation by photon energy are both are responsible for the increase in optical conductivity.

Optical Properties of SnO₂ 277

Table 3. SnO ₂ thin-layer optical properties over the vis-band at 500 nm	
	_

Thicknesses (nm) (t)			Optical pro	perties over	the Vis-spectr	al area at "5	00 nm"		
	T	A	α(1/cm)	R	k	n	3	ε	σ
510	0.90	0.04	1915.10	0.051	0.0076	1.58	2.5	0.024	0.00061
630	0.86	0.06	2267.54	0.071	0.0090	1.72	2.98	0.031	0.00085
770	0.84	0.07	2154.65	0.081	0.0085	1.79	3.22	0.030	0.00077
940	0.80	0.096	2355.19	0.102	0.0095	1.941	3.76	0.036	0.00093





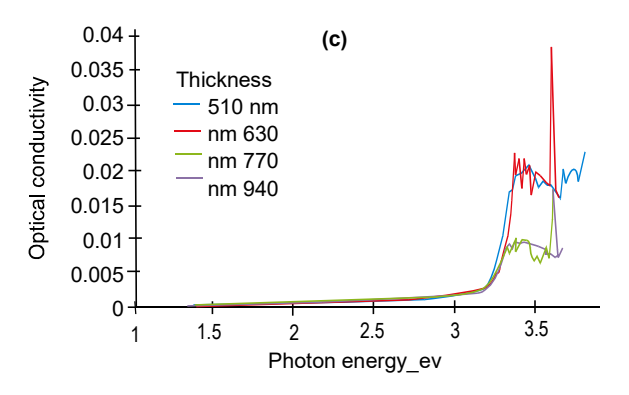


Fig. 6. (a) Urbach energy (b) Skin depth (nm) (c)
Optical conductivity of SnO₂ layers.

Conclusion

Chemical spray pyrolysis "CSP" has been successfully used to create thin layers of SnO₂. The properties of optically thin layers were studied. According to the findings, the optical energy gap for a permitted direct electronic transition was observed to decrease from 3.29 to 3.21 (eV) and from 3 to 2.9 eV for a permitted direct and indirect electronic transition, with an increase in the thickness of the film. Every thin layer exhibits low in transmittance in the UV-region, which increases as the wave-length increases toward the near-infrared region. In addition, the films exhibit a good interference pattern in terms of transmittance, which is a sign of improved homogeneity and high quality. The investigation into the effect of thin layer thickness on optical properties has demonstrated that alterations in the thickness of thin layers exert a profound influence on a comprehensive range of optical parameters. These parameters include absorption and extinction coefficients, refractive index, as well as the real and imaginary parts of the dielectric constant.

Acknowledgement

My thanks and appreciation to the laboratories of the University of Baghdad and the Ministry of Science and Technology for completing the requirements of this study.

Conflict of Interest. The authors declare that they have no conflict of interest.

References

Abdullah, D., Al-Taay, H. 2021. Structure, morphology and optical properties of SnO₂ nanoparticle synthesized *via* ultrasonic spray pyrolysis technique: effect of CuO doping concentration. *Journal of Physics: Conference Series*, **2114**: 012074. DOI 10.1088/1742-6596/2114/1/012074

Billur, C., Gencosman. 2020. The effect of films

- thickness on structural and optical properties of amorphous SnO₂ thin films deposited by ink jet printing method. *Journal of Molecular Structure*, **1219:** 128577. https://doi.org/10.1016/j.molstruc. 2020.128577
- Brunin, G., Ricci, F. 2019. Transparent conducting materials discovery using high-throughput computing. *NPJ Computational Materials*, **5:** 1-13. https://doi.org/10.1038/s41524-019-0200-5
- Carreno, N., Rangel, J. 2003. Effect of the structures on the optical properties of (PbLa)TiO₃ thin films. Bulgarian Journal of Physics, **30:** 131-140. http://www.bjp-bg.com/papers/bjp2003 3-4 131-140.pdf
- Chen, Z., Wang, X. 2013. Nano indentation of porous bulk and thin films of La0.6Sr0.4Co0.2Fe0.8O3-δ. *Acta Materialia*, **61:** 5720-5734. https://doi.org/10.1016/j.actamat.2013.06.016
- Erken, Ö., Gümü°, C. 2018. Determination of the thickness and optical constants of polycrystalline SnO₂ thin film by envelope method. *Adiyaman University Journal of Science*, **8:** 141-151.
- Farva, U., Kim, J. 2021. Growth temperature-dependent morphological, optical and electrical study of SnO₂ thin film by atomic layer deposition. *Materials Chemistry and Physics*, **267**: 124584. https://doi.org/10.1016/j.matchemphys.2021.124584
- Hasaean, A., Akl, A. 2015. Influence of composition on optical and dispersion parameters of thermally evaporated non-crystalline Cd₅₀S₅₀-_xSe_x thin films. *Journal of Alloys and Compounds*, **648**: 280-290. https://doi.org/10.1016/j.jallcom.2015.06.231
- Khamee, W., Niyom, K. 2023. Thickness dependence of optical properties of sputtered AZO film on borosilicate glass. *Journal of Physics: Conference Series*, **2653**: 012046. DOI: 10.1088/1742-6596/2653/1/012046
- Korber, C., Harvey, S. 2008. Barrier heights at the SnO₂/Pt interface: *In situ* photoemission and electrical properties. *Surface Science*, **602**: 3246-3252. https://doi.org/10.1016/j.susc.2008.08.015 Kumar, R., Kaphle, G. 2023. Unraveling the structural

- and mechanical stability, electronic and optical properties of (LaxSr1-xVO3)n (n=1,2; x=0,0.5,1). *Solid State Communications*, **368**: 115173. https://doi.org/10.1016/j.ssc.2023.115173
- Lei Ma, H., Hao, X.-T. 2002. Thickness dependence of properties of SnO₂:Sb films deposited on flexible substrates. *Applied Surface Science*, **191**: 313-318. https://doi.org/10.1016/S0169-4332(02)00253-2
- Paliwal, A., Sharma, A. 2014. Dielectric properties of SnO₂ thin film using SPR technique for gas sensing applications. *Conference Papers in Science*, 7: 1-4. http://dx.doi.org/10.1155/2014/656120
- Sarmah, S., Kumar, A. 2010. Optical properties of SnO₂ nanoparticles. *Indian Journal of Physics*, **84:** 1211-1221. DOI: 10.1007/s12648-010-0109-9
- Susilawati, Muliyadi. 2020. The thickness effect to optical properties of SnO₂ thin film with doping fluorine. *Journal of Physics Conference Series*, **1572:** 012085. http://dx.doi.org/10.1088/1742-6596/1572/1/012085
- Torre Pari, D., Aquino, J. 2023. Enhancing the photoconductivity and gas sensing performance of TiO₂/SnO₂ hetero structures tuned by the thickness of the SnO₂ upper layer. *Applied Surface Science*, **613:** 156028. https://doi.org/10.1016/j.apsusc.2022. 156028
- Yadav, A.A., Masumdar, E.U., Moholkar, A.V., Neumann-Spallart, M.K.Y. 2009. Electrical, structural and optical properties of SnO₂:F thin films: Effect of the substrate temperature. *Journal of Alloys and Compounds*, **488**: 350-355. https://doi.org/10.1016/j.jallcom.2009.08.130
- Yan, M., Zhang, Q. 2015. Applications of transparent conducting oxides in organic light emitting devices. *Journal of Nanoscience and Nanotechnology*, 15: 6279-6294. https://doi.org/10.1166/jnn.2015.10732
- Zhang, W., Li, J., Xing, Y., Nie, X., Lang, F., Yang, S., Hou, X., Zhao, C. 2021. Experimental study on the thickness-dependent hardness of SiO₂ thin films using nanoindentation. *Coatings*, **11:** 23. https://doi.org/10.3390/coatings11010023